Atmos. Chem. Phys. Discuss., 11, 23421–23468, 2011
www.atmos-chem-phys-discuss.net/11/23421/2011/
doi:10.5194/acpd-11-23421-2011

Atmospheric Chemistry and Physics Discussions

Parameterising secondary organic aerosol from α-pinene using a detailed oxidation and aerosol formation model

K. Ceulemans, S. Compernolle, and J.-F. Müller

Belgian Institute for Space Aeronomy (BIRA-IASB), Brussels, Belgium

Received: 14 March 2011 – Accepted: 1 August 2011 – Published: 18 August 2011

Correspondence to: K. Ceulemans (karl.ceulemans@aeronomie.be)

Published by Copernicus Publications on behalf of the European Geosciences Union.

Abstract

A new 10-product parameter model for α-pinene secondary organic aerosol (SOA) is presented, based on simulations with the detailed model BOREAM (Biogenic hydrocarbon Oxidation and Related Aerosol formation Model). The parameterisation takes into account the influence of temperature, type of oxidant, NO_x-regime, photochemical ageing and water uptake, and is suitable for use in global chemistry transport models. BOREAM is validated against recent photooxidation smog chamber experiments, for which it reproduces SOA yields to within a factor of 2 in most cases. In the simple chemical mechanism of the parameter model, oxidation of α-pinene generates peroxy radicals, which, upon reaction with NO or HO_2, yield products corresponding to high or low-NO_x conditions, respectively. The model parameters – i.e. the temperature-dependent stoichiometric coefficients and partitioning coefficients of the 10 semi-volatile products – are obtained from simulations with BOREAM, including a prescribed diurnal cycle for the radiation, oxidant and emission levels, as well as a deposition sink for the particulate and gaseous products. The effects of photooxidative ageing are implicitly included in the parameterisation, since it is based on near-equilibrium SOA concentrations, obtained through simulations of a two-week period. Modelled SOA mass yields are about ten times higher in low-NO_x than in high-NO_x conditions, with yields of about 50 % in the low-NO_x OH-initiated oxidation of α-pinene, considerably more than in previous parameterisations based on smog chamber experiments. The parameterisation is only moderately sensitive to the assumed oxidant levels. However, photolysis of species in the particulate phase is found to strongly reduce SOA yields. Water uptake is parameterised using fitted activity coefficients, resulting in a good agreement with the full model.

ACPD
11, 23421–23468, 2011

1 Introduction

Aerosols play an important role in the Earth's atmosphere through their impact on climate (Solomon et al., 2007) and air quality (Pope III et al., 2002; Krewski et al., 2009). Organic material often makes up more than 50 % of atmospheric aerosols, of which an important fraction is secondary organic aerosol (SOA), containing semi-volatile gas phase oxidation products of volatile organic compounds (VOC), that partition between the gas and aerosol phase (Jimenez et al., 2009). Several VOC have been identified as important SOA precursors through smog chamber experiments, such as aromatic compounds, mostly of anthropogenic origin (Ng et al., 2007b), and biogenic species such as the monoterpenes (for examples, see references in Sect. 2.5), sesquiterpenes (Ng et al., 2007a), isoprene (Kroll et al., 2006) and dicarbonyls (Volkamer et al., 2009).

The monoterpene α-pinene is one of the volatile organic compounds whose SOA formation mechanism has received most attention. Numerous smog chamber studies have been conducted, aimed at monitoring SOA yields and elucidating the gas phase and aerosol phase composition and chemical mechanisms, which were either "dark ozonolysis" (see for example the experiments cited in Table 1 in Ceulemans et al. (2010)) or "photooxidation" experiments (see Sect. 2.5).

Experimental results have been combined with structure-activity relationships, and sometimes theoretical quantum-level calculations (Peeters et al., 2001), to construct detailed mechanisms for the gas phase oxidation of α-pinene, which have been supplemented with a partitioning model (Kamens and Jaoui, 2001; Jenkin, 2004; Capouet et al., 2008; Xia et al., 2008). Such detailed mechanisms are often too large for use in global chemistry transport models, however. Moreover, these models still contain many uncertainties (Hallquist et al., 2009), which can lead to discrepancies between modelled and experimental SOA yields (Xia et al., 2008; Ceulemans et al., 2010).

Another approach towards SOA modelling has been the direct fitting of parameterised two-product models for SOA formation against experimental SOA mass yields (Odum et al., 1996), and for α-pinene a number of parameterisations has been derived

ACPD
11, 23421–23468, 2011

(see Sect. 3.5). Most smog chamber experiments were hitherto conducted under conditions which, for one or more aspects, differ from those which can be found in the atmosphere: initial VOC loadings are often higher, NO_x concentrations might differ, OH-scavengers might be used, and their run-time is often relatively short – several hours – while atmospheric photochemical ageing might continue for several days. Parameterisations based on experimental studies lack some of the sensitivity to important factors, such as NO_x regime or ageing, due to lack of reliable experimentally determined yields at various experimental configurations, or because such effects were simply ignored in the parameterisation.

A number of global modelling studies on SOA formation have made use of SOA parameterisations for various precursors (see for example Henze et al., 2008; Tsigaridis and Kanakidou, 2007; Farina et al., 2010; Pye and Seinfeld, 2010; Pye et al., 2010; Carlton et al., 2010). Biogenic precursors, and in particular the monoterpenes, are found to be major contributors to SOA, but a consensus on the contributions of the various types of organic aerosol, and on its total global production, has not been reached yet, with large differences between different models, and with measurements, remaining. In such studies, parameterisations for α-pinene SOA are often used as a proxy for SOA from some or all of the monoterpenes.

Various factors can impact SOA yields. Increasing temperature is expected to have a decreasing effect, by increasing the saturated vapour pressure of semi-volatile compounds. SOA parameterisations (Odum et al., 1996; Presto et al., 2005a) based on SOA experiments around the same temperature do not contain an explicit temperature dependence. In Pathak et al. (2007) dark α-pinene experiments at temperatures between 15 and 40 °C were conducted, and a decrease in SOA yields was observed with increasing temperature, which was smaller than the decrease predicted by the full BOREAM model (Ceulemans et al., 2010), however. Saathoff et al. (2009) conducted a large number of dark ozonolysis experiments at different temperatures, and explicitly included the temperature dependence in their parameterisation. Several global modelling studies have made use of an estimated enthalpy of vaporisation (ΔH_{vap}),

ACPD
11, 23421–23468, 2011

to account for the temperature dependence of SOA yields (Chung and Seinfeld, 2002; Henze et al., 2008; Farina et al., 2010; Pye and Seinfeld, 2010). The estimated ΔH_{vap} is still quite uncertain, but its impact on global SOA production is large, especially outside the boundary layer (Henze and Seinfeld, 2006; Farina et al., 2010). The temperature sensitivity in the parameterisation of Stanier et al. (2008) is based on an enthalpy of vaporisation derived from chamber experiments at different temperatures.

Photochemical ageing can have a strong impact on SOA composition and yields. Long-term oxidation of semi-volatile compounds by OH was shown to be crucial (Jimenez et al., 2009). However, most previous parameterisations were based on chamber studies using OH-scavengers, and/or on experiments which did not last more than a few hours. Some recent studies have tried to remedy the absence of ageing impact on parameterised SOA yields through the use of a volatility basis set, which allows oxidation products to evolve through reactions with OH (Lane et al., 2008; Jimenez et al., 2009; Farina et al., 2010). These ageing parameterisations are still quite uncertain: they may require a number of arbitrary choices (for example the change in volatility upon reaction), as these models are still not fully constrained by adequate experimental results under atmospheric conditions. In the most recent global modelling studies (e.g. Farina et al., 2010; Pye et al., 2010) the impact of long-term ageing was ignored for biogenic VOCs.

Whereas Tsigaridis et al. (2006) only considered ozonolysis as a significant SOA source, photooxidation experiments, such as Ng et al. (2007a) indicated that high SOA yields are also found in the OH-initiated oxidation of α-pinene, especially under low-NO_x conditions. Most global modelling studies use identical SOA yields for ozonolysis and OH-oxidation (Chung and Seinfeld, 2002; Farina et al., 2010; Pye et al., 2010). Experimentally it is difficult to fully separate the SOA yields due to these oxidants. In dark ozonolysis experiments, an OH scavenger limits the oxidation of α-pinene to ozonolysis, but this also limits ageing through OH-oxidation. In photooxidation experiments, significant ozone levels might be present, which oxidise part of the VOC.

ACPD
11, 23421–23468, 2011

SOA yields from α-pinene have been shown to decrease with increasing NO_x concentrations (Presto et al., 2005a; Ng et al., 2007a; Capouet et al., 2008), although the same is not necessarily true for other VOCs, such as sesquiterpenes (Ng et al., 2007a) and isoprene (Hoyle et al., 2011). Presto et al. (2005a) and Pathak et al. (2007) provided separate high and low-NO_x SOA yield parameterisations. Until recently, NO_x dependence was not considered for biogenic species in most global models. Farina et al. (2010) and Pye et al. (2010) have employed a parameterisation with a NO_x dependence for the monoterpenes, however, which follows the approach of Henze et al. (2008) for aromatics.

Simulations indicate that water uptake by SOA can significantly increase SOA yields at high relative humidities (Xia, 2006; Compernolle et al., 2009). Measured growth factors show that water can be taken up in significant amounts by SOA (Meyer et al., 2009), although Engelhart et al. (2011) found only slight increases of total aerosol volume due to SOA water uptake from measurements at Crete. Water uptake by SOA has been ignored in most global modelling studies, however, due to lack of reliable and easily implementable parameterisations.

In this paper, we present a 10-product parameterisation for α-pinene SOA, taking into account the impact of temperature, type of oxidant, NO_x-regime and photochemical ageing on SOA yields. The effect of water uptake is also treated. Due to its small size, this parameterisation is easily implementable in global chemistry transport models. The parameterisation is based on simulations with the detailed model BOREAM (Capouet et al., 2008; Ceulemans et al., 2010). The use of a box model makes it possible to easily cover a wide range of photochemical conditions. The parameterisation is designed to reproduce the SOA yields at equilibrium, when SOA formation is balanced by deposition losses, after typically two weeks. A similar approach was adopted recently in Xia et al. (2011), in which a reduced mechanism, containing a volatility basis set with further ageing reactions, was designed, based on simulations with the detailed MCM mechanism for α-pinene.

ACPD
11, 23421–23468, 2011

Section 2 presents the BOREAM model, in particular its generic chemistry mechanism (Sect. 2.2), which represents the further-generation chemistry. The model is validated against a number of photooxidation smog-chamber studies in Sect. 2.5. Next, in Sect. 3.1 the parameter model is presented, and the adjustment of its parameters is described in Sect. 3.2. In Sect. 3.4 the sensitivity of the parameterised SOA to NO_x, HO_x and radiation levels is investigated. Section 3.5 presents a comparison with previous parameterisations. Finally, in Sect. 3.6, the treatment of water uptake is discussed.

2 Full box model description

2.1 Gas phase chemistry mechanism

The gas phase mechanism of the BOREAM model is described in Capouet et al. (2008). The chemistry of the radical reactions, up to primary products is based on advanced quantum chemical calculations for key reactions (Peeters et al., 2001; Vereecken et al., 2007; Capouet et al., 2008; Ceulemans et al., 2010), and on structure activity relationships (SARs) for other primary gas phase reactions. The cross reactions of peroxy radicals are represented through reactions with counter species representing different peroxy radical classes.

Further chemistry of the primary products includes photolysis and reaction with OH, ozone or NO_3, which are based as much as possible on recent structure activity relationships (Capouet et al., 2008). The further generation products are lumped into so-called semi-generic and generic species classes (Capouet et al., 2008; Ceulemans et al., 2010). The semi-generic species are classes defined by their carbon number and by their functional groups, whereas their precise structure is not specified. Only the most common secondary products are described through the semi-generic scheme, as a complete description would require a prohibitively large number of categories.

ACPD
11, 23421–23468, 2011

2.2 Generic chemistry

The generic chemistry system was introduced in Capouet et al. (2008), and further extended in Ceulemans et al. (2010). Generic species are used to represent classes of lumped multi-functional compounds. In the current version of the model, generic species are defined by their carbon number (from 10 down to 6) and by one explicit functional group. Other functional groups which might be present in the multi-functional compounds which the generic species represents, are not explicitly rendered. These "implicit" functional groups still have an impact on the volatility and reactivity of the compound. Therefore the generic species are further subdivided into 11 volatility classes. Each class represents lumped organic compounds, which have a "parent compound" (the molecule resulting from replacement of the explicit functional group by one or more hydrogen atoms) with a saturated liquid vapour pressure $p^0_{\mathrm{L,parent}}$ falling within the volatility class range. For the highest volatility class, indicated by the letter "a", $p^0_{\mathrm{L,parent}} > 10^{-1}$ Torr at 298 K. Class "b" contains species with 10^{-1} Torr $> p^0_{\mathrm{L,parent}} > 10^{-1.5}$ Torr, etc., and for class "k", $p^0_{\mathrm{L,parent}} < 10^{-5.5}$ Torr.

In the model, the non-radical generic species themselves are then assigned a vapour pressure, determined by the contribution of its explicit group (based on Capouet and Müller, 2006), and the representative volatility class vapour pressure $p^0_{\mathrm{L,LX}}$, taken to be equal to the geometric mean of the volatility class range for classes "b"–"j", $10^{-0.75}$ Torr for class "a", and $10^{-5.75}$ Torr for class "k".

In our notation a generic species name consists of the prefix "LX", the carbon number, the vapour pressure class symbol and the explicit functional group. In total there are 55 classes (5 carbon numbers times eleven vapour pressure classes), besides the generic products with less than 6 carbon atoms, which are not considered for SOA formation, and lumped into a special generic class (with prefix "SX").

Each class includes 13 gas phase species: 3 radical species (alkoxy, peroxy and acyl peroxy) and 10 molecular species, and their chemistry is described by 86 reactions for each class (see Supplementary Material).

ACPD
11, 23421–23468, 2011

Molecular generic compounds can react with the OH radical or undergo photolysis. The rates of reactions involving the explicitly represented functional group are obtained through structure activity relationships, as for the explicit molecular products. In order to account for the reactivity of the implicit part of the generic compounds, we assume that generic species with lower vapour pressures are more functionalised, and therefore generally more reactive. On the basis of simple assumptions, described in the Supplementary Material, the OH-reactivity and photolysis rates have been assigned.

Whereas reactions such as photolysis or alkoxy-radical decomposition lead to a loss of carbon atoms or functional groups from the molecule, other reactions might add functional groups to the implicit part of the molecule. In each case, the product of the reaction is assigned to the appropriate carbon number/volatility class.

The generic alkoxy radicals can undergo three types of reactions (Table 1): reaction with O_2, leading to a carbonyl function (1), decomposition (2) or isomerisation (3).

The reaction with O_2 usually has a reaction rate of the order $3–8\times10^4\ s^{-1}$, and is not strongly dependent on the structure of the alkoxy radical, in contrast with the reaction rates for decomposition or H-shift isomerisation (see Vereecken and Peeters, 2009, 2010). Three types of decomposition are considered: decomposition into an alkyl radical and CH_2O, when the alkoxy radical is primary; formic acid elimination, when the alkoxy radical contains an alcohol group; and acetone elimination. Other types of decomposition, for example breaking of a ring structure, are not considered.

The branching ratio estimates are based on the reactions of the explicit alkoxy radicals present in BOREAM (see Capouet et al., 2004, 2008). It is found that decomposition occurs in most cases, followed by H-shift isomerisation. Decomposition of alkoxy radicals is favoured by the presence of oxygenated functional groups (Vereecken and Peeters, 2009). It is therefore assumed that lower volatility compounds, which generally have more functional groups, have a higher branching towards decomposition. Among the decompositions, type (2.a) (Table 1) is most common.

The implicit part of the generic species changes upon decomposition or H-shift isomerisation. In particular, the product generally belongs to a different volatility class than

ACPD
11, 23421–23468, 2011

the reactant. This is illustrated with two examples from Table 1.

In Reaction (2.c), the reactant loses three carbon atoms and one alcohol functionality, leading to an expected increase of $p^0_{\mathrm{L,parent}}$ of 3.5 orders of magnitude, according to the vapour pressure method used in our model (Capouet and Müller, 2006). Since one vapour pressure class spans a $\log(p^0_{\mathrm{L,parent}})$ range of 0.5, the product in our example moves up 7 volatility classes, from class "i" to class "b".

On the other hand, for H-shift isomerisation (Reaction (R3) in Table 1) the alkoxy radical abstracts an H-atom from another carbon, leading to a hydoxy alkyl radical (Vereecken and Peeters, 2010). This radical can react with oxygen, forming a peroxy radical, which becomes the explicitly represented group. The alcohol function is included in the implicit part of the generic species, reducing its volatility, so that it moves to the lowest vapour pressure class "k". Besides reactions with O_2, the intermediate hydroxy alkyl radical might contain a primary carbonyl function, in which case it becomes an acyl peroxy radical ("LX10kO3"), or it might contain an α-hydroperoxide, nitrate or alcohol function, in which cases it decomposes into an aldehyde. The implicit part of the generic species then loses a functional group, so that product volatility is increased ("LX10gCHO").

For peroxy- and acyl peroxy radicals, the same scheme as for explicit (acyl-)peroxy radicals is used, where we assign to all alkyl peroxy radicals the reactivity of secondary alkyl peroxy radicals (the "R2R" class defined in Capouet et al. (2008)).

The generic chemistry contains the implicit representation of a very large number of chemical reactions which the further generation products are expected to undergo. It is based on choices for rate constants, made on the basis of analogy with other mechanisms, such as the explicit primary chemistry of α-pinene. The assumed reactivity of the implicit part of the generic species remains, however, among the largest sources of uncertainty in our model.

ACPD
11, 23421–23468, 2011

2.3 Heterogeneous and aerosol phase chemistry

Studies have pointed towards the importance of heterogeneous and aerosol phase chemistry. Although the formation of peroxy hemiacetals was investigated in a sensitivity test using BOREAM (Capouet et al., 2008), the reaction rates remain quite uncertain, and this reaction is not part of the current version of BOREAM. Other oligomer forming reactions, such as hemiacetal formation and esterification have been proposed, but the reaction rates of these processes, which often require acid catalysis in the aerosol phase, are still not known (see Hallquist et al. (2009) for an overview). Other studies have focused on OH-oxidation of the aerosol phase (Smith et al., 2009). This process is neglected, as sensitivity tests indicate that it only has a minor impact on SOA yields due to kinetic limitations under atmospheric conditions (Hildebrandt et al., 2010).

In previous modelling studies, the photolysis of species in the aerosol phase was generally ignored, due to a lack of data, and because the further chemistry of radical products in the aerosol is poorly understood. Several recent studies have shown that photolysis of oxygenated organic compounds in the particulate phase is far from negligible. In Mang et al. (2008) the photolysis of carbonyls in limonene SOA was investigated, and estimates of the quantum yield and absorption spectra for the carbonyl compounds in the SOA led to an estimated lifetime of about 6 hours for a zenith angle of 20°. The present model version includes aerosol phase photolysis, with identical J-values and product distributions as in the gas phase, in view of the lack of more reliable experimental data.

2.4 Partitioning between gas phase and aerosol phase

The partitioning between aerosol and gas phase is treated as in Ceulemans et al. (2010). It makes use of the absorption theory of Pankow (1994), in which the equilibrium constant $K_{p,i} = C_{p,i}/C_{g,i} \cdot M_O^{-1}$ determines the ratio of the particle and gas phase concentration of species i, which is also dependent on the total absorbing organic

ACPD
11, 23421–23468, 2011

aerosol mass concentration M_O (in $\mu g\,m^{-3}$). This partitioning constant can be calculated through the formula

$$K_{p,i} = \frac{760 \cdot RT \cdot f_{om}}{MW_{om} \cdot 10^6 \cdot \gamma_i \cdot p^0_{L,i}} \quad (1)$$

where R is the gas constant ($atm\,m^3\,K^{-1}\,mol^{-1}$); T is temperature (K); MW_{om} is the molecular weight of the absorbing medium ($g\,mol^{-1}$); f_{om} is the weight fraction of organic matter in the total aerosol; γ_i is the activity coefficient of compound i in the particulate phase; $p^0_{L,i}$ is its subcooled saturated vapour pressure (here in Torr); 760 ($Torr\,atm^{-1}$) and 10^6 ($\mu g\,g^{-1}$) are unit conversion factors. The method of Capouet and Müller (2006) is used to estimate the vapour pressure $p^0_{L,i}$ as a function of temperature for the semi-volatile species present in the BOREAM gas phase mechanism. The activity coefficients γ_i are calculated online using the method described in Compernolle et al. (2009), covering most relevant atmospheric functional groups. It is an adapted version of UNIFAC (Fredenslund et al., 1975), as formulated by Hansen et al. (1991), and with some parameters determined by Raatikainen and Laaksonen (2005). Water uptake is also considered by the model.

2.5 Model comparison against photooxidation smog chamber experiments

Previous simulations of α-pinene photooxidation (Capouet et al., 2008) and dark ozonolysis (Ceulemans et al., 2010) smog chamber experiments showed that the BOREAM SOA mass yields generally fall within a factor two of the experimental data. For dark ozonolysis, larger discrepancies were found at high temperatures (above 30 °C) and at low VOC loadings and no seed. In this section, the current version of the BOREAM model (updated for generic chemistry, aerosol photolysis, water uptake and non-ideality effects) is evaluated, with a focus on photooxidation experiments, and on experiments in which secondary chemistry through OH-oxidation or photolysis takes place.

ACPD
11, 23421–23468, 2011

An overview of the simulated experiments is given in Table 2. All experiments made use of a light source. Most experiments also included a considerable quantity of NO_x, except the first two experiments of Ng et al. (2007a), which were conducted under very low-NO_x conditions, and three of the Presto et al. (2005a) experiments considered. For experiment 1 in Ng et al. (2007a), unknown quantities of NO_x, H_2O_2 and O_3 were present at the start of the experiment, which were constrained using the measurements of α-pinene and O_3 for this experiment, provided in Valorso et al. (2011), following the approach of this last study. For experiment 4 in Ng et al. (2007a), the HONO concentration and an unknown OH-source were constrained similarly, based on α-pinene and NO_x data (see again Valorso et al., 2011). For the low-NO_x scenario, reasonable agreement is reached for ozone production (see Fig. 2 in the Supplement). For the high-NO_x experiment, reproducing the observed α-pinene decay is possible only when an additional OH-source is included, possibly due to reactions on walls, as proposed by Valorso et al. (2011). Reasonable agreement is obtained with measured NO and NO_2 concentrations (see Fig. 5 in the Supplement). However, for one intermediate-NO_x experiment, serious overestimations of ozone production were found, both in Valorso et al. (2011) and in our study. It is doubtful that SOA yields can be simulated reliably when the model shows such discrepancies for ozone. Therefore we did not include this experiment in the overview in Table 2. SOA yields for this experiment were actually strongly overestimated, as in Valorso et al. (2011). In addition, we show simulations of three experiments of Carter (2000), in which the quantity $D(O_3 - NO) = ([O_3] - [O_3]_{initial}) - ([NO] - [NO]_{initial})$ was determined experimentally. The current BOREAM model version shows good agreement or slight overestimation of ozone production for these experiments (see Figs. 7 to 9 in the Supplement).

In Ng et al. (2007a) an aerosol density of $1.32\,g\,cm^{-3}$ was measured, which was used to derive the experimental mass yields, based on the experimentally determined aerosol volume concentrations. A density of $1.25\,g\,cm^{-3}$ was used by Ng et al. (2006). In all other studies considered, measured SOA volume concentrations were transformed into mass concentrations based on an assumed aerosol density of $1.0\,g\,cm^{-3}$.

ACPD
11, 23421–23468, 2011

Since this estimate is likely too low, in view of the measurement of Ng et al. (2007a), we have multiplied the reported SOA mass yields by a factor of 1.32.

In Fig. 1, modelled and experimental SOA mass yields are compared. For most experiments, the SOA yields are reproduced well within a factor of 2. The overestimations of more than a factor 2 found for three experiments of Takekawa et al. (2003) might be related to uncertainties regarding the yield of some carboxylic acids, such as pinic and hydroxy pinonic acid, which are formed in α-pinene ozonolysis, but for which the formation mechanism is not well understood (Ceulemans et al., 2010). Their production yield is held fixed in the model, although it is very probably dependent on photochemical conditions, e.g. the NO_x abundance. In some experiments, such as Takekawa et al. (2003) and Hoffmann et al. (1997), there is a considerable ozone production, so that part of the α-pinene undergoes ozonolysis (besides reaction with OH). The model reproduces well the SOA decrease with increasing NO_x concentrations, as seen from the comparison of experiments 1 and 4 of Ng et al. (2007a), for which the time evolution is given in Figs. 3 and 6 in the Supplement. The SOA yield in the low-NO_x experiment 1 of Ng et al. (2007a) is overestimated by the model, a result which was also obtained in Valorso et al. (2011). Overall the model results agree reasonably well with the experimental values, considering the theoretical and experimental uncertainties.

3 Parameterised SOA formation model based on BOREAM

3.1 Parameterised 10-product model

In contrast to previous mechanism reduction studies (e.g. Xia et al., 2009), which aimed at reproducing the impact of the precursor VOC not only on SOA formation but also on the concentrations of oxidants and several key gaseous compounds, we limit the scope of our parameterisation to SOA formation as modelled by BOREAM in typical atmospheric conditions. For this purpose, we adopt the commonly used two-product model first applied by Odum et al. (1996), except that the parameters are obtained

ACPD
11, 23421–23468, 2011

from box model simulations with BOREAM, and that the parameterisation accounts for the dependence of SOA yields on the nature of the oxidant (OH, O_3 or NO_3) and on the abundance of NO. This leads us to consider 5 different scenarios: OH-oxidation and ozonolysis, both for low and high-NO_x, and high-NO_x NO_3-oxidation. It is found that in each case 2 condensable products suffice to parameterise SOA-formation, thus leading to a model containing in total 10 condensible products.

In the original two-product model, oxidation of the SOA precursor leads to the immediate formation of two surrogate compounds, with mass-stoichiometric coefficients (α_i) and partitioning constants ($K_{p,i}$) adjusted in order to reproduce a set of experimental SOA yields, through the equation

$$Y = \sum Y_i = M_O \sum \frac{\alpha_i K_{p,i}}{1 + K_{p,i} \cdot M_O} \quad (2)$$

where Y is the SOA mass yield. Note that the molar stoichiometric coefficients α'_i can be derived from the mass-stoichiometric coefficients and the ratio of the molar mass of the precursor and the organic aerosol: $\alpha'_i = MW_{\alpha\text{-pinene}}/MW_{OA} \cdot \alpha_i$. In order to account for the large influence of the NO_x-regime on SOA yields (see for example Presto et al., 2005b or Capouet et al., 2008), the VOC oxidation product can be taken to be a peroxy radical ("PRAPOH1" and "PRAPO31", see Table 3), which upon reaction with NO or HO_2, leads to a set of condensable products with stoichiometric and partitioning coefficients adjusted against experiments conducted under high or low NO conditions respectively. This system, adopted by Henze et al. (2008) to parameterise NO_x-dependence of SOA yields for aromatic compounds, is also used here, although modified with the introduction of an additional peroxy radical ("PRAPOH2" or "PRAPO32" in Table 3), in order to better reproduce the NO_x-dependence of the yields at intermediate NO levels, as described in more detail in Sect. 3.4.1. The reduced mechanism of our parameterisation is presented in Table 3. Note that the reaction of α-pinene with NO_3 is assumed to be unimportant in low-NO_x conditions, so that the condensable products can be formed immediately from this reaction. The parame-

ACPD
11, 23421–23468, 2011

terisation includes a total of 11 equations and 10 condensable products. Note that, although the cross-reactions of peroxy radicals are ignored in the reduced mechanism, their role is taken into account in the full BOREAM model. This simplification is not expected to cause large errors, except in the case of very high VOC loadings.

3.2 Scenarios for full model runs

The parameters of the 10-product model are obtained from full BOREAM model simulations conducted under five scenarios, each corresponding to one pair of products. We limit the oxidation of α-pinene to one oxidant, by turning off the reactions with the other two main oxidants. All oxidants, however, are allowed to react with the oxidation products of α-pinene. For the high-NO_x scenario we adopt a concentration of 100 ppb NO_2, while for the low-NO_x scenario we take 1 ppt of NO_2.

In order to mimic real atmospheric conditions, where SOA is composed of a mix of fresh and aged material, subject to wet and dry deposition, we conduct BOREAM simulations including a sustained emission of α-pinene, as well as a sink of gaseous and particulate compounds due to dilution and deposition. Adopting a sink term corresponding to a lifetime of 6 days, typical for organic aerosols (see for example Farina et al., 2010), as well as prescribed diurnal cycles for the photolysis rates and for the concentrations of OH, HO_2, O_3, α-pinene and NO_2, the system approaches a quasi-steady-state in about 12 days. The noontime photolysis rates are calculated by assuming a 20° zenith angle. Their diurnal variation is assumed to follow a $\sin^2$ function zeroing at 05:00 LT and 19:00 LT, corresponding to summertime conditions at mid-latitudes. The concentrations of OH and HO_2 are kept constant during the night, at 2×10^5 and 10^8 cm^{-3}, respectively, whereas their noontime (maximum) values are set to 10^7 and 2×10^9 cm^{-3}, respectively. These values are in the range of concentrations reported from field measurements, e.g. Hofzumahaus et al. (2009) in the Pearl River Delta, Martinez et al. (2003) around Nashville, and Martinez et al. (2010) in the Surinam rainforest.

ACPD
11, 23421–23468, 2011

Ozone concentrations are also prescribed, and follow a diurnal cycle. For high-NO_x scenarios or when O_3 is the main oxidant, the night-time concentrations are assumed to be 15 ppb, and during the day they follow the diurnal cycle, reaching a maximum value of 60 ppb. In low-NO_x conditions, and when OH is the oxidant, ozone concentrations typical of unpolluted areas are chosen with 5 ppb at night and 15 ppb at the daytime maximum.

For each simulation, the quasi-steady state SOA yield is calculated from the model results on the last day of the simulation, with Y = [OA produced]/[α-pinene consumed]. Assuming equilibrium, [OA produced] is equal to the loss through deposition during one day, which equals the daily averaged aerosol concentration divided by the lifetime in days. A series of runs with increasing VOC concentrations is then performed, in order to cover a range of organic aerosol loadings between about 0.1 and 50–100 $\mu g\,m^{-3}$. Water uptake to the aerosol phase is suppressed in these runs. The additional SOA formation due to water uptake will be parameterised through activity coefficients, as documented in Sect. 3.6.

In order to take the temperature sensitivity of the yields into account, $Y(M_O)$ curves are obtained at seven temperatures between 273 K and 303 K, with steps of 5 K. We assume the following temperature dependence for the partitioning constant:

$$K_{p,i}(T) = K_{p,i}(T_r)\frac{T}{T_r}\exp\left(\frac{\Delta H_i}{R}\left(\frac{1}{T}-\frac{1}{T_r}\right)\right)\frac{\mathrm{MW}}{\mathrm{MW_{ref}}} \quad (3)$$

in which the reference temperature T_r = 298 K, ΔH_i represents the enthalpy of vaporisation and $\mathrm{MW_{ref}}$ is the reference average molar mass of the molecules in the SOA. This approach was followed by Saathoff et al. (2009) for obtaining temperature-dependent coefficients for α-pinene dark ozonolysis experiments over a wide range of temperatures. Equation (3) can be rewritten as $K_{p,i}(T) = A_i \cdot T \cdot \exp(\frac{B_i}{T})$, where A_i and B_i are the fitting parameters. For the mass stoichiometric coefficient, a temperature dependence of the form

$$\alpha_i(T) = \alpha_i^0 \exp(\alpha_i^1 (T - T_r)) \quad (4)$$

ACPD
11, 23421–23468, 2011

is assumed.

3.3 Parameter adjustment results

The parameterisations are obtained by minimising the relative difference between the box model yields and the yields calculated using Eq. (2). Comparison of the fitted and full model (see Fig. 2 and the Supplementary Material file) shows a satisfactory agreement in most cases, to better than 10 % for nearly all data points in the range 0.5–50 $\mu g\,m^{-3}$. Figure 3 shows the parameterised $Y(M_O)$ curves at 298 K between 0 and 20 $\mu g\,m^{-3}$. For both low-NO_x scenarios, yields are about a factor 10 higher than the high-NO_x yields. The reduction of SOA yields at high-NO_x has been observed in several previous experimental studies, such as Presto et al. (2005a). The yields for the OH-oxidation of α-pinene are found to be somewhat higher than for ozonolysis, in both NO_x regimes. The yields for NO_3-oxidation are quite small at 298 K, but the yields for this scenario increase significantly at lower temperatures. The yield curves for the high-NO_x scenarios lie quite close to each other, and their maximum in this range is about 3–4 %. In Table 4, the fitted parameters for the ten products considered are given.

3.4 Sensitivity of the parameterised yields to model assumptions

Since photochemical conditions in the atmosphere might differ from the conditions assumed for the parameterisation, in this subsection we investigate the sensitivity of the parameterised yields to key parameters and assumptions.

3.4.1 NO_x dependence

The NO_x dependence of the parameterised model is based on full model runs at very high and very low NO_x levels. As seen in Table 3, the parameterisation involves two peroxy radicals ("PRAPOH1" and "PRAPOH2") upon α-pinene oxidation by OH, and

ACPD
11, 23421–23468, 2011

two peroxy radicals ("PRAPO31" and "PRAPO32") upon α-pinene ozonolysis. A simpler parameterisation similar to the scheme used in Henze et al. (2008), in which only one peroxy radical was produced (i.e. when the branching ratio towards the second-generation peroxy radicals "PRAPOH2" and "PRAPO32" is zero), has been tested, but was found to lead to significant SOA overestimates at intermediate NO_x levels. This can partly be explained by the fact that the peroxy radicals reacting with HO_2 in the parameter model immediately yield highly condensable low-NO_x products, which in the full model correspond to products formed after several subsequent reactions of peroxy radicals with HO_2, for example hydroxy dihydroperoxides. In the full model, however, a reaction with HO_2 can be followed by a reaction with NO, leading to the formation of a much more volatile product.

The introduction of the additional peroxy radicals "PRAPOH2" and "PRAPO32", as seen in Table 3, results in a redistribution between high and low-NO_x products, and to an improved agreement between full and parameter model at intermediate NO_x levels for both OH and ozone oxidation (see Fig. 4, and Fig. 14 in the Supplement). We have also checked the agreement of full and parameter model at intermediate-NO_x levels at different temperatures (see Figs. 15 to 18 in the Supplement), for which deviations from the full model remain within 10–15 % at most atmospherically relevant SOA loadings.

Note that even at high NO_x or low NO_x, small discrepancies persist between parameter model and full model. For the high-NO_x scenario, an overestimation is found, due to the fact that some peroxy radicals react with HO_2 during the night, even at elevated NO_2 concentrations, yielding low volatility "low-NO_x" products. The SOA underestimation at low NO_x (1 ppt NO_2) is caused by the longer time needed to reach equilibrium in the parameterisation (about 40 days). Parameter model yields shown here were sampled after 24 days. This discrepancy is only a few percent at most, however.

3.4.2 Importance of aerosol photolysis for SOA ageing

Aerosol photolysis has only little impact for the simulation of the experiments described in Table 2, which lasted only a few hours. Aerosol photolysis has, however, a poten-

ACPD
11, 23421–23468, 2011

tially major impact on SOA yields after prolonged ageing. In the full model simulations, described in Sect. 3.2, turning off aerosol photolysis leads to a very strong increase of the SOA yields, in particular for the oxidation of α-pinene by OH under low-NO_x conditions, with SOA mass yields reaching values of around 100 % (see Fig. 5, magenta full curve).

This strong sensitivity of SOA yields to aerosol photolysis after several days of ageing is caused by the fact that most condensable species, formed in the oxidation of α-pinene, reside predominantly in the aerosol phase. When photolysis of the aerosol phase species is ignored, only the small fraction of these condensable species left in the gas phase can undergo further reactions (photolysis or oxidation by OH). The more volatile species, residing mostly in the gas phase, are oxidised in part to low-volatility compounds, which can move towards the aerosol phase, where they are shielded from further oxidation. This process will over time lead to an accumulation of very condensable oxidation products in the SOA.

Aerosol photolysis can partly revolatilise these condensable species, except those which do not contain any photolabile chromophore. Ignoring aerosol photolysis will therefore likely lead to unrealistically high SOA yields in models, although large uncertainties exist, regarding the rates of aerosol phase photolysis reactions. Further experimental work is clearly desirable.

In a second sensitivity test, the solar zenith angle used in the calculation of photorates, is increased from 20° to 45° (but the prescribed oxidant levels are kept identical, however). This leads to an increase of SOA yields (dashed magenta curve), e.g. from 0.48 to 0.58 at $M_O = 10\,\mu g\,m^{-3}$.

3.4.3 Influence of assumed OH and HO_2 concentrations

OH and HO_2 play an important role in SOA formation, especially at low NO_x, since their concentrations determine the formation of hydroperoxides and other oxygenetated species. As seen in Fig. 5, the SOA yields increase by up to about 0.03, when the OH and HO_2 concentrations are doubled.

ACPD
11, 23421–23468, 2011

Halving the OH and/or HO_2 levels leads to comparatively larger changes. E.g. at $M_O = 10\,\mu g\,m^{-3}$, the SOA yield at low-NO_x is reduced from 0.48 to 0.41 when both the OH and HO_2 concentrations are halved. In conclusion, the use of a fixed diurnal profile for OH and HO_2 in the model calculations introduces small but significant uncertainty in the parameterised SOA formation rate, typically of the order of 10–15 %.

3.5 Comparison with parameterised models based on experimental yields

A non-exhaustive overview of parameterisations for SOA formation from α-pinene based on smog chamber studies is given in Table 5.

Figure 6 compares the SOA yield curves for these studies with the parameterisation obtained with BOREAM. The reference temperature is taken to be 298 K, to allow for proper comparison. For those experimental parameterisations which do not contain an explicit temperature dependence, we adjusted the partitioning equilibrium constants by use of Eq. (3), assuming a value for $\Delta H_{vap}/R$ of 5000 K, although it should be noted that a large uncertainty exists for the enthalpy of vaporisation of SOA (Stanier et al., 2008). For the parameterisation of Hoffmann et al. (1997) this adjustment nearly doubles the SOA yield, but for most other parameterisations the difference is less important.

Figure 6 shows a very large variation between the different parameterisations based on experiments, stressing the large impact of experimental conditions on the SOA yields. Most experimental SOA yield curves fall between the high yields of the low-NO_x BOREAM results and the low yields for the high-NO_x scenario.

Low-NO_x model scenario yields are considerably higher than those for the experimental studies, partly due to the fact that in the model scenarios ageing has a larger impact. These model scenarios assume an average lifetime of 6 days for the gas and aerosol species, much longer than the duration of the smog chamber experiments, which typically last several hours. Moreover, in most ozonolysis studies, OH scavengers were used, which limits the extent of further ageing which the primary products can undergo. In the low-NO_x model scenario, the continuous exposure of products to OH and HO_2 is responsible for much of the increase in functionalisation (with for

ACPD
11, 23421–23468, 2011

example additional hydroperoxide groups as a result) and decrease in volatility of the oxidation products. In shorter experiments, or in experiments without OH, this process will be limited, and SOA yields remain low.

The high-NO_x curve for Presto et al. (2005a) agrees well with the high-NO_x BOREAM scenarios. In the BOREAM simulations with high-NO_x photooxidation the reaction with NO yields mostly alkoxy radicals, and some nitrates or peroxy acyl nitrates (PANs) as side products. The alkoxy radicals can in some cases decompose, which leads to smaller carbon chains or to a loss of oxygenated functional groups, increasing volatility. This explains the large difference found between high and low-NO_x yields, and also why long-term ageing under high-NO_x conditions might lead to lower SOA yields than seen in high-NO_x SOA experiments of shorter duration. As an illustration, the high-NO_x experimental yields of Ng et al. (2007a) are shown in Fig. 6. These yields are higher than in the BOREAM scenario for photooxidation at high-NO_x. It should be noted that in the simulation of these experiments, the full BOREAM model calculated SOA yields comparable to the experimental SOA yields (see Fig. 1).

Experimental SOA parameterisations for α-pinene have been used in several global modelling studies, where they are generally used to represent SOA from the monoterpene family. Pye et al. (2010) used a NO_x-dependent parameterisation, for which the low-NO_x yield is based on the study of Shilling et al. (2008), which consisted of dark ozonolysis experiments with addition of an OH scavenger. The absence of OH can partly explain their lower yield compared to BOREAM.

In Farina et al. (2010), a NO_x-dependent parameterisation using a 4-product volatility basis set was used, based on the studies of Hoffmann et al. (1997), Ng et al. (2006) and Ng et al. (2007a). Their high-NO_x yields lie somewhat higher than the high-NO_x experimental yields of Ng et al. (2007a) and the temperature-adjusted parameterisation of Hoffmann et al. (1997). Their low-NO_x curve is considerably lower than the low-NO_x experimental yield of Ng et al. (2007a), and the low-NO_x BOREAM yield curve.

ACPD
11, 23421–23468, 2011

3.6 Treatment of water uptake and water activity

In Compernolle et al. (2009) the UNIFAC method for activity coefficient calculation, as implemented by Hansen et al. (1991), was extended to include missing atmospherically relevant functional groups, such as the hydroperoxide, peroxy-acid, nitrate and peroxy acyl nitrate groups. This method was applied in all BOREAM simulations presented in this study. However, water uptake was not considered in these simulations, although it is expected to increase the total number of molecules in the absorbing phase, and therefore also the partitioning to the particulate phase of organic semi-volatile compounds.

These effects are included in our parameterisation through the introduction of an activity coefficient for water, γ_{H_2O}, and a pseudo-activity coefficient for the organics in SOA, γ_{Org}. Both parameters are estimated from BOREAM simulations including water uptake, conducted at a temperature of 298 K and at relative humidity values ranging between 0.5 and 99.5 % with a step of 1 %.

As a simplification, the SOA is treated as a binary mixture of water and one organic pseudo-compound, which represents the entire organic fraction of the SOA. The overall pseudo-activity coefficient γ_{Org} accounts for the non-ideality effects which the added water exerts on the organic compounds, whereas the non-ideality effects among organic compounds are implicitly accounted for in the parameterisation without water uptake.

Figure 7 shows the resulting dependence of the water activity coefficient on relative humidity. At relatively low relative humidity (typically below 60 %), the water activity coefficient is lower than 1, leading to an increased water concentration in SOA, compared to the ideal case, in which the relative molecular water concentration would be equal to the relative humidity. γ_{H_2O} reaches a maximum of 1.08 for the low-NO_x scenario at 92% RH. At 100 % RH, γ_{H_2O} is equal to 1, which is expected, as the organic fraction becomes very small, causing non-ideality effects of the organic fraction to become negligible.

ACPD
11, 23421–23468, 2011

Two methods are used to derive the pseudo-activity coefficient γ_{Org} f or the organic fraction. In the first method, γ_{Org} is obtained from the modelled activity coefficient and molecular fraction of water in SOA. Indeed, for a binary mixture, when the molar fraction and activity coefficient for one component are known, the Gibbs-Duhem relationship at constant temperature and pressure (Poling et al., 2001)

$$x_1 \left(\frac{\partial \ln \gamma_1}{\partial x_1} \right)_{T,P} = x_2 \left(\frac{\partial \ln \gamma_2}{\partial x_2} \right)_{T,P} \quad (5)$$

might be used to derive the activity coefficient of the other component through an integration. At $x_1 = 0$, the activity coefficient of the second component is 1, and $\ln \gamma_2 = 0$. We can then integrate Eq. (5) from $x_1 = 0$ to any x_1 (Olander, 2007):

$$\int_{\ln \gamma_2(x_1=0)}^{\ln \gamma_2(x_1)} d \ln \gamma_2 = \ln \gamma_2 = - \int_{\ln \gamma_1(x_1=0)}^{\ln \gamma_1(x_1)} \frac{x_1}{1 - x_1} d \ln \gamma_1 \quad (6)$$

Taking water and the organic fraction to be component 1 and 2, $\gamma_2 = \gamma_{Org}$ can be obtained by the numerical evaluation of the integral on the right-hand side of Eq. (6), with γ_1 and x_1 provided by BOREAM model simulations.

Figure 8 shows the resulting γ_{Org} decreases from a value of 1 at 0 % RH to a minimum of 0.4-0.6 at about 92–95 % RH (depending on the scenario), above which γ_{Org} increases rapidly. The two low-NO_x scenarios have comparable γ_{H_2O} and γ_{Org} curves, as well as the three high-NO_x scenarios.

Comparing the SOA yields of the parameter model (with the above obtained activity coefficients) and the full model (Fig. 9), a good agreement is found for the low-NO_x OH-oxidation. For the high-NO_x scenario, however, the use of the Gibbs-Duhem γ_{Org} leads to larger deviations above 50% RH. Therefore, for high-NO_x conditions a direct optimisation of γ_{Org} was performed instead, at 160 RH values between 0 and 100%, which minimises the difference in M_O between full and parameterised model (shown in black in Fig. 8). As can be seen in Fig. 9, these values lead to an excellent agreement of the SOA yields for the high-NO_x scenario. Tabulated values for γ_{H_2O} and γ_{Org} for

ACPD
11, 23421–23468, 2011

OH-oxidation can be found in Table 8 (for low-NO_x) and Table 9 (for high-NO_x) of the Supplementary Material.

Sensitivity tests in which the activity coefficients are given constant values (1 or 1.1 for γ_{H_2O}, and 1 for the organic species) show that at high RH the use of these constant values for the γ can lead to important discrepancies (Fig. 9).

Extrapolation to intermediate NO_x levels of the above parameterisation for water uptake and water activity can be performed as follows. γ_{Org} is extrapolated by assigning the values of $\gamma_{Org,low-NO_x}$ and $\gamma_{Org,high-NO_x}$ to respectively low- and high-NO_x products in the SOA. γ_{H_2O} is extrapolated based on the mass fraction of low-NO_x products in the SOA, r_{low-NO_x}, using $\gamma_{H_2O} = \left(\gamma_{H_2O,low-NO_x}\right)^{r_{low-NO_x}} \times \left(\gamma_{H_2O,high-NO_x}\right)^{(1-r_{high-NO_x})}$. We have performed simulations at intermediate NO_x (100 ppt and 1 ppb NO_2), showing that the agreement between full and parameter model deteriorates slightly, but discrepancies still remain limited to 10–15 % (see Fig. 19 in the Supplement). This agreement is reasonable, given that the typical model uncertainty on SOA yields and loadings is usually higher.

4 Conclusions

The detailed model BOREAM is used to simulate the formation of SOA accompanying α-pinene oxidation under near-atmospheric conditions, including continued photochemical ageing.

The chemistry of further generation oxidation products is represented by a generic chemistry scheme, which is described in detail. Photolysis of species in the aerosol phase is included, in analogy with gas phase photolysis. Evaluation against a large number of photooxidation smog chamber experiments shows that most experimental SOA mass yields can be reproduced to within a factor 2.

BOREAM is used to design an SOA parameterisation for use in large-scale atmospheric models. The oxidation of α-pinene by OH, ozone and NO_3 are modelled sep-

ACPD
11, 23421–23468, 2011

arately. Simulations are performed with BOREAM for high- and low-NO_x conditions, using a prescribed diurnal cycle for radiation, oxidants and α-pinene, while deposition of gas phase and particulate compounds is considered. The equilibrium SOA mass concentrations, reached typically after about 12 days, are used to constrain the parameters (temperature-dependent mass stoichiometric coefficients and partitioning constants) of the 10-product model. It is shown to reproduce the SOA formation of the full BOREAM model reasonably well at all NO_x levels. A strong decrease of SOA mass yields is found for increasing NO_x concentrations.

The SOA mass yields are shown to be relatively insensitive to variations of the concentrations of OH and HO_2 adopted in the simulations. Increasing radiation intensity reduces SOA mass yields considerably, however (at similar oxidant levels). The photolysis of aerosol phase species has a large impact on the SOA mass yields in atmospheric conditions, since it is found to reduce SOA yields by a factor of about 2 after several days of ageing in the low-NO_x OH-initiated oxidation scenario. Particulate phase photolysis is therefore a large factor of uncertainty which warrants further experimental studies.

The low-NO_x SOA mass yields in our model are found to be considerably higher (up to 50 % mass yield for low-NO_x OH-oxidation) than in previously published SOA parameterisations based on smog chamber experiments. This is largely due to the fact that these smog chamber experiments were not conducted at the very low NO_x concentrations (1 ppt) used in our model, and generally did not allow for much photochemical ageing, in contrast with the simulations performed here. The simulated high-NO_x SOA yields, on the other hand, are found to be lower than in most experimental parameterisations.

The parameterisation of water uptake involves an RH-dependent activity coefficient for water, γ_{H_2O}, and an overall pseudo-activity coefficient γ_{Org}, which accounts for the non-ideality effects which the added water exerts on the organic compounds. Use of these adjusted activity coefficients in the parameterised model leads to a good agreement with the full model for all relative humidities, for both low and high-NO_x simula-

ACPD
11, 23421–23468, 2011

tions.

The parameterisation for secondary organic aerosol from α-pinene obtained in this work accounts for the influence of temperature, NO_x-regime, the impact of long-term photochemical ageing and water uptake, which was generally not the case for parameter models based on experiments, usually due to lack of sufficient data. It can therefore be used to estimate the impact of these factors in regional or global models, although large uncertainties remain, e.g. with respect to the photolysis of SOA and the further generation chemistry. Further model validation against long-term ageing experiments under various NO_x conditions is desirable. For wider application in SOA modelling it would also be necessary to extend this approach to other SOA precursors, and address the interaction with other types of aerosol components which might be present, such as primary organic aerosol or inorganic components.

Supplement related to this article is available online at: http://www.atmos-chem-phys-discuss.net/11/23421/2011/acpd-11-23421-2011-supplement.pdf.

Acknowledgements. This research has been made possible through funding to the IBOOT (SD/AT/03) and BIOSOA (SD/CS/05A) projects, which are part of the programme "Science for a Sustainable Development" (SSD) of the Belgian Science Policy Office (BELSPO), and through the Action-1 research grant MO/35/027 of BELSPO.

References

Capouet, M. and Müller, J.-F.: A group contribution method for estimating the vapour pressures of α-pinene oxidation products, Atmos. Chem. Phys., 6, 1455–1467, doi:10.5194/acp-6-1455-2006, 2006. 23428, 23430, 23432

Capouet, M., Peeters, J., Nozière, B., and Müller, J.-F.: α-pinene oxidation by OH: simulations of laboratory experiments, Atmos. Chem. Phys., 4, 2285–2311, doi:10.5194/acp-4-2285-2004, 2004. 23429, 23455

ACPD

11, 23421–23468, 2011

Capouet, M., Müller, J.-F., Ceulemans, K., Compernolle, S., Vereecken, L., and Peeters, J.: Modeling aerosol formation in α-pinene photooxidation experiments, J. Geophys. Res., 113, D02308, doi:10.1029/2007JD008995, 2008. 23423, 23426, 23427, 23428, 23429, 23430, 23431, 23432, 23435

Carlton, A. G., Bhave, P. V., Napelenok, S. L., Edney, E. O., Sarwar, G., Pinder, R. W., Pouliot, G. A., and Houyoux, M.: Model representation of secondary organic aerosol in CMAQv4.7, Environ. Sci. Technol., 44, 8553–8560, 2010. 23424

Carter, W. P. L.: Documentation of the SAPRC-99 chemical mechanism for VOC reactivity assessment, final report to California Resources Board, contracts 92-329 and 95-308, Tech. rep., Air Pollut. Res. Cent.for Environ. Res. and Technol., Univ. of California, Riverside, California, USA, http://.www.cert.ucr.edu/~carter/reactdat.htm, 2000. 23433

Ceulemans, K., Compernolle, S., Peeters, J., and Müller, J.-F.: Evaluation of a detailed model of secondary organic aerosol formation from alpha-pinene against dark ozonolysis experiments, Atmos. Environ., 40, 5434–5442, 2010. 23423, 23424, 23426, 23427, 23428, 23431, 23432, 23434

Chung, S. H. and Seinfeld, J. H.: Global distribution and climate forcing of carbonaceous aerosols, J. Geophys. Res., 107, 4407, doi:10.1029/2001JD001397, 2002. 23425

Cocker III, D. R., Clegg, S. L., Flagan, R. C., and Seinfeld, J. H.: The effect of water on gas-particle partitioning of secondary organic aerosol. Part I: α-pinene/ozone system, Atmos. Environ., 35, 6049–6072, 2001. 23459

Compernolle, S., Ceulemans, K., and Müller, J.-F.: Influence of non-ideality on condensation to aerosol, Atmos. Chem. Phys., 9, 1325–1337, doi:10.5194/acp-9-1325-2009, 2009. 23426, 23432, 23443

Engelhart, G. J., Hildebrandt, L., Kostenidou, E., Mihalopoulos, N., Donahue, N. M., and Pandis, S. N.: Water content of aged aerosol, Atmos. Chem. Phys., 11, 911–920, doi:10.5194/acp-11-911-2011, 2011. 23426

Farina, S. C., Adams, P. J., and Pandis, S. N.: Modeling global secondary organic aerosol formation and processing with the volatility basis set: Implications for anthropogenic secondary organic aerosol, J. Geophys. Res., 115, D09202, doi:10.1029/2009JD013046, 2010. 23424, 23425, 23426, 23436, 23442, 23459

Fredenslund, A., Jones, R. L., and Prausnitz, J. M.: Group-contribution estimation of activity-coefficients in nonideal liquid-mixtures, AIChE J., 21, 1086–1099, 1975. 23432

Griffin, R. J., Flagan, R. C., and Seinfeld, J. H.: Organic aerosol formation from the oxidation

ACPD
11, 23421–23468, 2011

of biogenic hydrocarbons, J. Geophys. Res., 104, 3555–3567, doi:10.1029/1998JD100049, 1999. 23459

Hallquist, M., Wenger, J. C., Baltensperger, U., Rudich, Y., Simpson, D., Claeys, M., Dommen, J., Donahue, N. M., George, C., Goldstein, A. H., Hamilton, J. F., Herrmann, H., Hoffmann, T., Iinuma, Y., Jang, M., Jenkin, M. E., Jimenez, J. L., Kiendler-Scharr, A., Maenhaut, W., McFiggans, G., Mentel, T. F., Monod, A., Prvt, A. S. H., Seinfeld, J. H., Surratt, J. D., Szmigielski, R., and Wildt, J.: The formation, properties and impact of secondary organic aerosol: current and emerging issues, Atmos. Chem. Phys., 9, 5155–5236, doi:10.5194/acp-9-5155-2009, 2009. 23423, 23431

Hansen, H. K., Rasmussen, P., Fredenslund, A., Schiller, M., and Gmehling, J.: Vapor-liquid-equilibria By UNIFAC group contribution. 5. Revision and extension, Ind. Eng. Chem. Res., 30, 2352–2355, 1991. 23432, 23443

Henze, D. K. and Seinfeld, J. H.: Global secondary organic aerosol from isoprene oxidation, Geophys. Res. Lett., 33, L09812, doi:10.1029/2006GL025976, 2006. 23425

Henze, D. K., Seinfeld, J. H., Ng, N. L., Kroll, J. H., Fu, T.-M., Jacob, D. J., and Heald, C. L.: Global modeling of secondary organic aerosol formation from aromatic hydrocarbons: high- vs. low-yield pathways, Atmos. Chem. Phys., 8, 2405–2420, doi:10.5194/acp-8-2405-2008, 2008. 23424, 23425, 23426, 23435, 23439

Hildebrandt, L., Kostenidou, E., Mihalopoulos, N., Worsnop, D. R., Donahue, N. M., and Pandis, S. N.: Formation of highly oxygenated organic aerosol in the atmosphere: Insights from the Finokalia Aerosol Measurement Experiments, Geophys. Res. Lett., 37, L23801, doi:10.1029/2010GL045193, 2010. 23431

Hoffmann, T., Odum, J. R., Bowman, F., Collins, D., Klockow, D., Flagan, R. C., and Seinfeld, J. H.: Formation of organic aerosols from the oxidation of biogenic hydrocarbons, J. Atmos. Chem., 26, 189–222, 1997. 23434, 23441, 23442, 23456, 23459

Hofzumahaus, A., Rohrer, F., Lu, K., Bohn, B., Brauers, T., Chang, C.-C., Fuchs, H., Holland, F., Kita, K., Kondo, Y., Li, X., Lou, S., Shao, M., Zeng, L., Wahner, A., and Zhang, Y.: Amplified trace gas removal in the troposphere, Science, 324, 1702, doi:10.1126/science.1164566, 2009. 23436

Hoyle, C., Boy, M., Donahue, N. M., Fry, J. L., Glasius, M., Guenther, A., Hallar, A. G., Huff Hartz, K., Petters, M. D., Petj, T., Rosenoern, T., and Sullivan, A. P.: A review of the anthropogenic influence on biogenic secondary organic aerosol, Atmos. Chem. Phys., 11, 321–343, doi:10.5194/acp-11-321-2011, 2011. 23426

ACPD

11, 23421–23468, 2011

Jenkin, M.: Modelling the formation and composition of secondary organic aerosol from α- and β-pinene ozonolysis using MCM v3, Atmos. Chem. Phys., 4, 1741–1757, doi:10.5194/acp-4-1741-2004, 2004. 23423

Jimenez, J. L., Canagaratna, M. R., Donahue, N. M., Prevot, A. S. H., Zhang, Q., Kroll, J. H., DeCarlo, P. F., Allan, J. D., Coe, H., Ng, N. L., Aiken, A. C., Docherty, K. S., Ulbrich, I. M., Grieshop, A. P., Robinson, A. L., Duplissy, J., Smith, J. D., Wilson, K., Lanz, V. A., Hueglin, C., Sun, Y. L., Tian, J., Laaksonen, A., Raatikainen, T., Rautiainen, J., Vaattovaara, P., Ehn, M., Kulmala, M., Tomlinson, J. M., Collins, D. R., Cubinson, M. J., Dunlea, E. J., Huffman, J. A., Onasch, T. B., Alfarra, M. R., Williams, P. I., Bower, K., Kondo, Y., Schneider, J., Drewnick, F., Borrmann, S., Weimer, S., Demerjian, K., Salcedo, D., Cottrell, L., Griffin, R. Takami, A., Miyoshi, T., Hatakeyama, S., Shimono, A., Sun, J. Y., Zhang, Y. M., Dzepina, K., Kimmel, J. R., Sueper, D., Jayne, J. T., Herndon, S. C., Trimborn, A. M., Williams, L. R., Wood, E. C., Middlebrook, A. M., Kolb, C. E., Baltensperger, U., and Worsnop, D. R.: Evolution of organic aerosols in the atmosphere, Science, 326, 1525–1529, doi:10.1126/science.1180353, 2009. 23423, 23425

Kamens, R. and Jaoui, M.: Modeling aerosol formation from α-pinene + NO_x in the presence of natural sunlight using gas-phase kinetics and gas-particle partitioning theory, Environ. Sci. Technol., 35, 1394–1405, 2001. 23423

Krewski, D., Jerrett, M., Burnett, R. T., Ma, R., Hughes, E., Shi, Y., Turner, M. C., Pope III, C. A., Thurston, G., Calle, E. E., and Thun, M. J.: Extended follow-up and spatial analysis of the American Cancer Society Study linking particulate air pollution and mortality, Tech. rep., Health Effects Institute, Boston, Massachusetts, USA, 2009. 23423

Kroll, J. H., Ng, N. L., Murphy, S. M., Flagan, R. C., and Seinfeld, J. H.: Secondary organic aerosol formation from isoprene photooxidation, Environ. Sci. Technol., 40, 1869–1877, 2006. 23423

Lane, T. E., Donahue, N. M., and Pandis, S. N.: Effect of NO_x on secondary organic aerosol concentrations, Environ. Sci. Technol., 41, 3984–3990, 2008. 23425

Mang, S. A., Henricksen, D. K., Bateman, A. P., Andersen, M. P. S., Blake, D. R., and Nizkorodov, S. A.: Contribution of carbonyl photochemistry to aging of atmospheric secondary organic aerosol, J. Phys. Chem. A, 112, 8337–8344, 2008. 23431

Martinez, M., Harder, H., Kovacs, T. A., Simpas, J. B., Bassis, J., Lesher, R., Brune, W. H., Frost, G. J., Williams, E. J., Stroud, C. A., Jobson, B. T., Roberts, J. M., Hall, S. R., Shetter, R. E., Wert, B., Fried, A., Alicke, B., Stutz, J., Young, V. L., White, A. B., and

ACPD
11, 23421–23468, 2011

Zamora, R. J.: OH and HO_2 concentrations, sources, and loss rates during the Southern Oxidants Study in Nashville, Tennessee, summer 1999, J. Geophys. Res., 108, 4617, doi:10.1029/2003JD003551, 2003. 23436

Martinez, M., Harder, H., Kubistin, D., Rudolf, M., Bozem, H., Eerdekens, G., Fischer, H., Klüpfel, T., Gurk, C., Königstedt, R., Parchatka, U., Schiller, C. L., Stickler, A., Williams, J., and Lelieveld, J.: Hydroxyl radicals in the tropical troposphere over the Suriname rainforest: airborne measurements, Atmos. Chem. Phys., 10, 3759–3773, doi:10.5194/acp-10-3759-2010, 2010. 23436

Meyer, N. K., Duplissy, J., Gysel, M., Metzger, A., Dommen, J., Weingartner, E., Alfarra, M. R., Prevot, A. S. H., Fletcher, C., Good, N., McFiggans, G., Jonsson, A. M., Hallquist, M., Baltensperger, U., and Ristovski, Z. D.: Analysis of the hygroscopic and volatile properties of ammonium seeded and unseeded SOA particles, Atmos. Chem. Phys., 9, 721–732, doi:10.5194/acp-9-721-2009, 2009. 23426

Ng, N. L., Kroll, J. H., Keywood, M. D., Bahreini, R., Varutbangkul, V., Flagan, R. C., Seinfeld, J. H., Lee, A., and Goldstein, A. H.: Contribution of first- versus second-generation products to secondary organic aerosols formed in the oxidation of biogenic hydrocarbons, Environ. Sci. Technol., 40, 2283–2297, 2006. 23433, 23442, 23456, 23459

Ng, N. L., Chhabra, P. S., Chan, A. W. H., Surratt, J. D., Kroll, J. H., Kwan, A. J., McCabe, D. C., Wennberg, P. O., Sorooshian, A., Murphy, S. M., Dalleska, N. F., Flagan, R. C., and Seinfeld, J. H.: Effect of NO_x level on secondary organic aerosol (SOA) formation from the photooxidation of terpenes, Atmos. Chem. Phys., 7, 5159–5174, doi:10.5194/acp-7-5159-2007, 2007a. 23423, 23425, 23426, 23433, 23434, 23442, 23456, 23459, 23465

Ng, N. L., Kroll, J. H., Chan, A. W. H., Chhabra, P. S., Flagan, R. C., and Seinfeld, J. H.: Secondary organic aerosol formation from m-xylene, toluene, and benzene, Atmos. Chem. Phys., 7, 3909–3922, doi:10.5194/acp-7-3909-2007, 2007b. 23423

Nozière, B., Barnes, I., and Becker, K. H.: Product study and mechanisms of the reactions of α-pinene and of pinonaldehyde with OH radicals, J. Geophys. Res.-Atmos., 104, 23645–23656, 1999. 23456

Odum, J. R., Hoffmann, T., Bowman, F., Collins, D., Flagan, R. C., and Seinfeld, J. H.: Gas/particle partitioning and secondary organic aerosol yields, Environ. Sci. Technol., 30, 2580–2585, 1996. 23423, 23424, 23434, 23459

Olander, D.: General Thermodynamics, CRC Press, 2007. 23444

Pankow, J. F.: An absorption model of gas/particle partitioning of organic compounds in the at-

ACPD
11, 23421–23468, 2011

mosphere, Atmos. Environ., 28, 185–188, doi:10.1016/1352-2310(94)90093-0, 1994. 23431
Pathak, R. K., Stanier, C. O., Donahue, N. M., and Pandis, S. N.: Ozonolysis of α-pinene at atmospherically relevant concentrations: Temperature dependence of aerosol mass fractions (yields), J. Geophys. Res.-Atmos., 112, D03201, doi:10.1029/2006JD007436, 2007. 23424, 23426
Peeters, J., Vereecken, L., and Fantechi, G.: The detailed mechanism of the OH-initiated atmospheric oxidation of α – pinene: a theoretical study, Phys. Chem. Chem. Phys., 3, 5489–5504, 2001. 23423, 23427
Poling, B. E., Prausnitz, J. M., and O'Connell, J. P.: The properties of gases and liquids, McGraw-Hill, 2001. 23444
Pope III, C. A., Burnett, R. T., Thun, M. J., Calle, E. E., Krewski, D., Ito, K., and Thurston, G. D.: Lung cancer, cardiopulmonary mortality, and long-term exposure to fine particulate air pollution, J. Am. Med. Assoc., 287, 1132–1141, 2002. 23423
Presto, A., Huff Hartz, K., and Donahue, N.: Secondary organic aerosol production from terpene ozonolysis. 2. Effect of NO_x concentration, Environ. Sci. Technol., 39, 7046–7054, 2005a. 23424, 23426, 23433, 23438, 23442, 23456, 23459
Presto, A. A., Hartz, K. E. H., and Donahue, N. M.: Secondary organic aerosol production from terpene ozonolysis. 1. Effect of UV radiation, Environ. Sci. Technol., 39, 7036–7045, 2005b. 23435
Pye, H. O. T. and Seinfeld, J. H.: A global perspective on aerosol from low-volatility organic compounds, Atmos. Chem. Phys., 10, 4377–4401, doi:10.5194/acp-10-4377-2010, 2010. 23424, 23425
Pye, H. O. T., Chan, A. W. H., Barkley, M. P., and Seinfeld, J. H.: Global modeling of organic aerosol: the importance of reactive nitrogen (NO_x and NO_3), Atmos. Chem. Phys., 10, 11261–11276, doi:10.5194/acp-10-11261-2010, 2010. 23424, 23425, 23426, 23442, 23459
Raatikainen, T. and Laaksonen, A.: Application of several activity coefficient models to water-organic-electrolyte aerosols of atmospheric interest, Atmos. Chem. Phys., 5, 2475–2495, doi:10.5194/acp-5-2475-2005, 2005. 23432
Saathoff, H., Naumann, K.-H., Mhler, O., Jonsson, . M., Hallquist, M., Kiendler-Scharr, A., Mentel, T. F., Tillmann, R., and Schurath, U.: Temperature dependence of yields of secondary organic aerosols from the ozonolysis of α-pinene and limonene, Atmos. Chem. Phys., 9, 1551–1577, doi:10.5194/acp-9-1551-2009, 2009. 23424, 23437, 23459
Shilling, J. E., Chen, Q., King, S. M., Rosenoern, T., Kroll, J. H., Worsnop, D. R., McKinney,

ACPD
11, 23421–23468, 2011

K. A., and Martin, S. T.: Particle mass yield in secondary organic aerosol formed by the dark ozonolysis of α-pinene, Atmos. Chem. Phys., 8, 2073–2088, doi:10.5194/acp-8-2073-2008, 2008. 23442, 23459

Smith, J. D., Kroll, J. H., Cappa, C. D., Che, D. L., Liu, C. L., Ahmed, M., Leone, S. R., Worsnop, D. R., and Wilson, K. R.: The heterogeneous reaction of hydroxyl radicals with sub-micron squalane particles: a model system for understanding the oxidative aging of ambient aerosols, Atmos. Chem. Phys., 9, 3209–3222, doi:10.5194/acp-9-3209-2009, 2009. 23431

Solomon, S., Qin, D., Manning, M., Chen, Z., Marquis, M., Averyt, K. B., Tignor, M., and Miller, H. L., eds.: Climate change 2007: the physical science basis, Cambridge University Press, 2007. 23423

Stanier, C. O., Donahue, N., and Pandis, S. N.: Parameterization of secondary organic aerosol mass fractions from smog chamber data, Atmos. Environ., 42, 2276–2299, 2008. 23425, 23441

Takekawa, H., Minoura, H., and Yamazaki, S.: Temperature dependence of secondary organic aerosol formation by photo-oxidation of hydrocarbons, Atmos. Environ., 37, 3413–3424, doi:10.1016/S1352-2310(03)00359-5, 2003. 23434, 23456

Tsigaridis, K. and Kanakidou, M.: Secondary organic aerosol importance in the future atmosphere, Atmos. Environ., 41, 4682–4692, 2007. 23424

Tsigaridis, K., Krol, M., Dentener, F. J., Balkanski, Y., Lathiere, J., Metzger, S., Hauglustaine, D. A., and Kanakidou, M.: Change in global aerosol composition since preindustrial times, Atmos. Chem. Phys., 6, 5143–5162, doi:10.5194/acp-6-5143-2006, 2006. 23425

Valorso, R., Aumont, B., Camredon, M., Raventos-Duran, T., Mouchel-Vallon, C., Ng, N. L., Seinfeld, J. H., Lee-Taylor, J., and Madronich, S.: Explicit modelling of SOA formation from α-pinene photooxidation: sensitivity to vapour pressure estimation, Atmos. Chem. Phys., 11, 6895–6910, doi:10.5194/acp-11-6895-2011, 2011. 23433, 23434

Vereecken, L. and Peeters, J.: Decomposition of substituted alkoxy radicals – part 1: a generalized structure-activity relationship for reaction barrier heights, Phys. Chem. Chem. Phys., 11, 9062–9074, 2009. 23429

Vereecken, L. and Peeters, J.: A structure-activity relationship for the rate coefficient of H-migration in substituted alkoxy radicals, Phys. Chem. Chem. Phys., 12, 12608–12620, 2010. 23429, 23430

Vereecken, L., Müller, J.-F., and Peeters, J.: Low-volatility poly-oxygenates in the OH-initiated

ACPD
11, 23421–23468, 2011

atmospheric oxidation of α-pinene: impact of non-traditional peroxyl radical chemistry, Phys. Chem. Chem. Phys., 9, 5241–5248, 2007. 23427

Volkamer, R., Ziemann, P. J., and Molina, M. J.: Secondary Organic Aerosol Formation from acethylene (C_2H_2): seed effect on SOA yields due to organic photochemistry in the aerosol aqueous phase, Atmos. Chem. Phys., 9, 1907–1928, doi:10.5194/acp-9-1907-2009, 2009. 23423

Xia, A. G., Michelangeli, D. V., and Makar, P. A.: Box model studies of the secondary organic aerosol formation under different HC/NO_x conditions using the subset of the Master Chemical Mechanism for α-pinene oxidation, J. Geophys. Res., 113, D10301, doi:10.1029/2007JD008726, 2008. 23423

Xia, A. G., Michelangeli, D. V., and Makar, P. A.: Mechanism reduction for the formation of secondary organic aerosol for integration into a 3-dimensional regional air quality model: alpha-pinene oxidation system, Atmos. Chem. Phys., 9, 4341–4362, doi:10.5194/acp-9-4341-2009, 2009. 23434

Xia, A. G., Stroud, C. A., and Makar, P. A.: Development of a simple unified volatility-based scheme (SUVS) for secondary organic aerosol formation using genetic algorithms, Atmos. Chem. Phys. Discuss., 11, 3885–3935, doi:10.5194/acpd-11-3885-2011, 2011. 23426

Xia, G.: Modeling secondary organic aerosol formation using a simple scheme in a 3-dimensional air quality model and performing systematic mechanism reduction for a detailed chemical mechanism, Ph.D. thesis, York University, Toronto, Ontario, 2006. 23426

ACPD
11, 23421–23468, 2011

Table 1. Illustration of generic alkoxy radical reactions included in BOREAM. R2R and RO3 denote peroxy radical counters (Capouet et al., 2004). The rates of these reactions are detailed in the Supplement.

$LX10iO + O_2 \rightarrow LX10iCHO + HO_2$ (1)
$LX10iO \rightarrow 0.60\ LX9hO_2 + 0.60\ R2R + 0.20\ LX9fO_3 + 0.20\ RO3 + 0.20\ LX9bCHO + 0.20\ OH + CH_2O$ (2.a)
$LX10iO \rightarrow LX9dO2 + R2R + HCOOH$ (2.b)
$LX10iO \rightarrow LX7bO2 + R2R + acetone$ (2.c)
$LX10iO \rightarrow 0.60\ LX10kO_2 + 0.60\ R2R + 0.20\ LX10kO_3 + 0.20\ RO_3 + 0.20\ LX10gCHO + 0.20\ OH$ (3)

ACPD
11, 23421–23468, 2011

Table 2. Photooxidation smog chamber experiments simulated with the full BOREAM model.

Experiment	Initial VOC (ppb)	NO_x (ppb)	Temperature (K)	NO_2 photolysis J-value (in s^{-1})	Exp. SOA mass yield	Model SOA mass yield
Ng et al. (2007a)						
Exp. 1	13.8	(0.7)	298	5.5×10^{-3}	0.379	0.592
Exp. 4	12.6	938	299	7.0×10^{-3}	0.066	0.070
Ng et al. (2006)						
Exp. 3/9/2005	108	95	293	1.1×10^{-3}	0.26	0.298
Presto et al. (2005a)						
Exp. 12	20.6	11	295	3.0×10^{-2}	0.065	0.066
Exp. 15	205	6.5	295	3.0×10^{-2}	0.304	0.331
Exp. 19	156	6	295	3.0×10^{-2}	0.251	0.284
Exp. 25	10.8	20	295	3.0×10^{-2}	0.026	0.019
Exp. 26	152	9	295	3.0×10^{-2}	0.224	0.278
Exp. 27	15	14	295	3.0×10^{-2}	0.057	0.040
Takekawa et al. (2003)						
Exp. 1	100	53	283	4.0×10^{-3}	0.312	0.390
Exp. 2	81	43	283	4.0×10^{-3}	0.317	0.360
Exp. 3	55	30	283	4.0×10^{-3}	0.275	0.307
Exp. 4	196	102	303	4.0×10^{-3}	0.133	0.249
Exp. 5	146	80	303	4.0×10^{-3}	0.119	0.224
Exp. 6	93	54	303	4.0×10^{-3}	0.066	0.187
Nozière et al. (1999)						
Exp. 17	305	3500	298	3.5×10^{-4}	0.073	0.067
Exp. 18	1488	3300	298	3.5×10^{-4}	0.306	0.314
Exp. 19	980	4090	298	3.5×10^{-4}	0.219	0.178
Exp. 20	330	3755	298	3.5×10^{-4}	0.079	0.102
Hoffmann et al. (1997)						
Exp. 3	72	203	315	8.3×10^{-3}(solar)	0.078	0.105
Exp. 4	19.5	113	315	8.3×10^{-3}(solar)	0.016	0.085
Exp. 5	53.0	206	324	8.3×10^{-3}(solar)	0.037	0.038
Exp. 6	94.5	135	321	8.3×10^{-3}(solar)	0.086	0.068
Exp. 7	87.4	125	321	8.3×10^{-3}(solar)	0.108	0.101
Exp. 8	95.5	124	316	8.3×10^{-3}(solar)	0.102	0.101
Exp. 9	94.6	122	316	8.3×10^{-3}(solar)	0.089	0.101

ACPD
11, 23421–23468, 2011

Table 3. Chemical mechanism of the parameterised 10-product model.

APIN + OH → PRAPOH1
PRAPOH1 + HO_2 → 0.5 α'_1 APOHL1 + 0.5 α'_2 APOHL2 + 0.5 PRAPOH2
PRAPOH2 + HO_2 → α'_1 APOHL1 + α'_2 APOHL2
PRAPOH2 + NO (or + NO_3) → α'_3 APOHH1 + α'_4 APOHH2
PRAPOH1 + NO (or + NO_3) → α'_3 APOHH1 + α'_4 APOHH2
APIN + O_3 → PRAPO31
PRAPO31 + HO_2 → 0.5 α'_5 APO3L1 + 0.5 α'_6 APO3L2 + 0.5 PRAPO32
PRAPO32 + HO_2 → α'_5 APO3L1 + α'_6 APO3L2
PRAPO32 + NO (or + NO_3) → α'_7 APO3H1 + α'_8 APO3H2
PRAPO31 + NO (or + NO_3) → α'_7 APO3H1 + α'_8 APO3H2
APIN + NO_3 → α'_9 APNO31 + α'_{10} APNO32

ACPD
11, 23421–23468, 2011

Table 4. Fitted parameters for the temperature-dependent 10-product model (5 scenarios considered).

Scenario	Product	α_i^0	α_i^1	$K_{p,i}(298)$ ($m^3 \mu g^{-1}$)	ΔH_i ($kJ\,mol^{-1}$)	MW_{ref} ($g\,mol^{-1}$)
α-pinene + OH, low-NO_x	APOHL1	0.341	−0.0217	9.23	77.2	216
	APOHL2	0.241	−0.0107	0.118	26.8	216
α-pinene + OH, high-NO_x	APOHH1	0.0277	−0.0521	1.30	119.9	253
	APOHH2	0.120	−0.0292	0.00812	74.1	253
α-pinene + O_3, low-NO_x	APO3L1	0.298	−0.0119	9.42	88.5	211
	APO3L2	0.160	−0.0223	0.0306	79.5	211
α-pinene + O_3, high-NO_x	APO3H1	0.0255	−0.0521	0.827	146.3	233
	APO3H2	0.215	−0.0104	0.00461	104.6	233
α-pinene + NO_3, high-NO_x	APNO31	0.0290	−0.0479	0.592	59.2	248
	APNO32	0.225	0.00038	0.00189	123.8	248

ACPD
11, 23421–23468, 2011

Table 5. Parameterisations for α-pinene SOA based on smog chamber experiments. VBS = Volatility Basis Set.

Study	Type	Oxidant	NO_x depend.	T depend.	Radiation
Odum et al. (1996)[a]	2-product	OH and O_3	no (intermediate NO_x)	no (±321 K)	solar
Griffin et al. (1999)	2-product	O_3 [d]	no (low NO_x)	no (308 K)	dark
Cocker III et al. (2001)	2-product	O_3 [d]	no (low NO_x)	no (301 K)	dark
Presto et al. (2005a)	2-product	O_3 [d]	yes (low and high NO_x)	no (295 K)	with/without UV
Saathoff et al. (2009)	2-product	O_3 [d]	no (low NO_x)	yes	dark
Pye et al. (2010)[b]	VBS	O_3 [d]	yes (low and high NO_x) $Y_{highNO_x} = \frac{1}{2} \cdot Y_{lowNO_x}$	no (298 K)	dark
Farina et al. (2010)[c]	VBS	OH and O_3	yes (low and high NO_x)	no	blacklight

[a] based on Hoffmann et al. (1997)
[b] based on Shilling et al. (2008)
[c] based on Hoffmann et al. (1997); Ng et al. (2006 , 2007a)
[d] including an OH-scavenger.

ACPD
11, 23421–23468, 2011

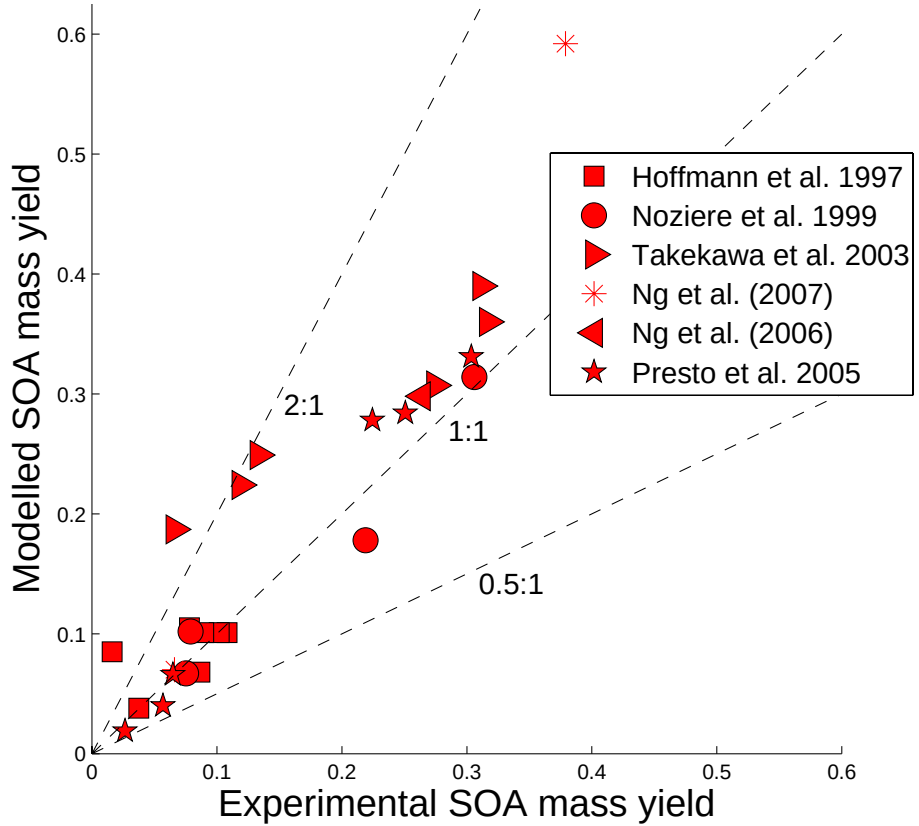

Fig. 1. Measured versus modelled aerosol mass yields for the α-pinene photooxidation smog chamber experiments reported in Table 2.

ACPD
11, 23421–23468, 2011

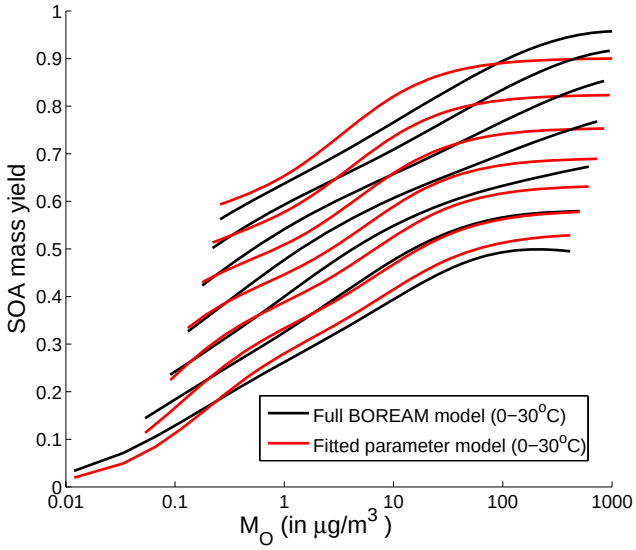

Fig. 2. Fitted and full model SOA mass yields as functions of the organic aerosol mass loading M_O, for the low-NO_x OH-oxidation scenario. The seven curves are obtained at temperatures ranging from 0 to 30 °C, by steps of 5 °C, the highest temperature corresponding to the lowest curve.

ACPD
11, 23421–23468, 2011

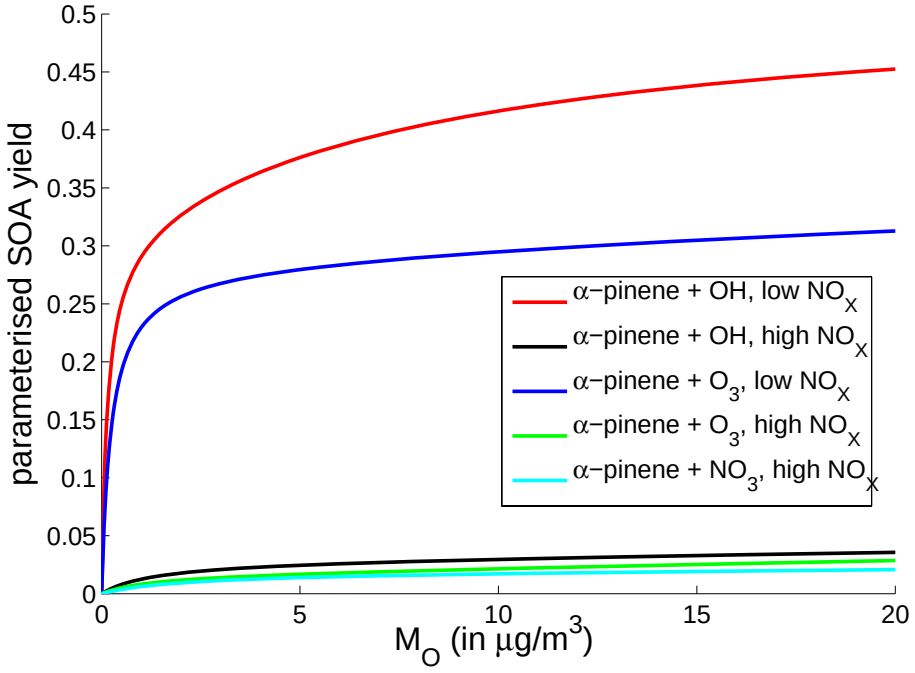

Fig. 3. Fitted SOA mass yields at 298 K for the five α-pinene oxidation scenarios, as functions of organic aerosol mass loading.

ACPD
11, 23421–23468, 2011

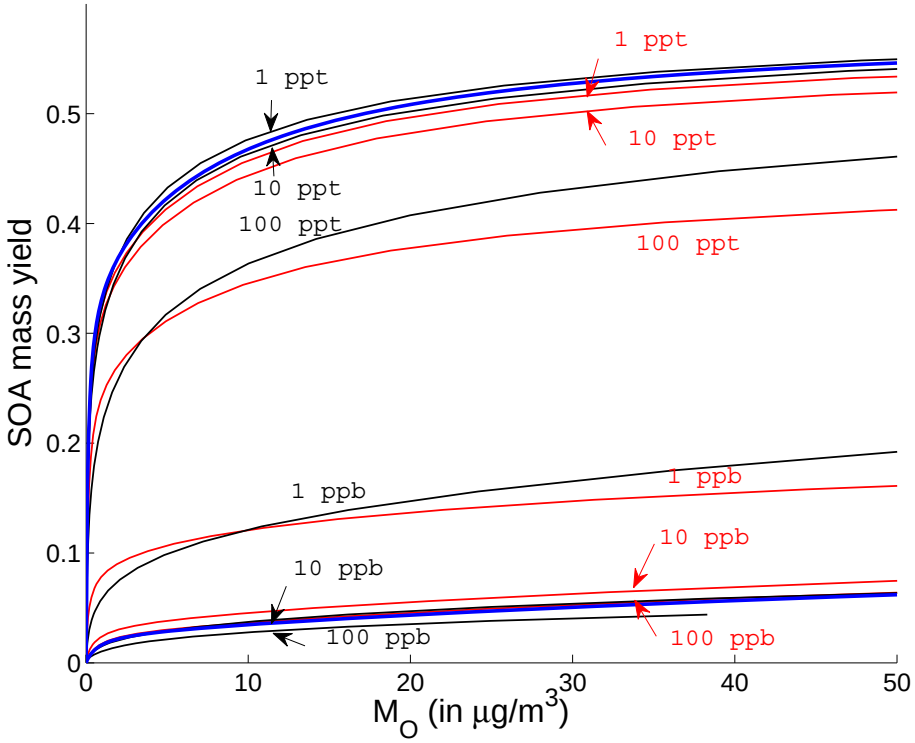

Fig. 4. SOA yields calculated by the full (black) and parameterised (red) model at NO_2 levels between 1 ppt and 100 ppb, for OH-oxidation of α-pinene (at 298 K). The parameterised functions $Y(M_O)$ for high and low-NO_x are shown in blue.

ACPD
11, 23421–23468, 2011

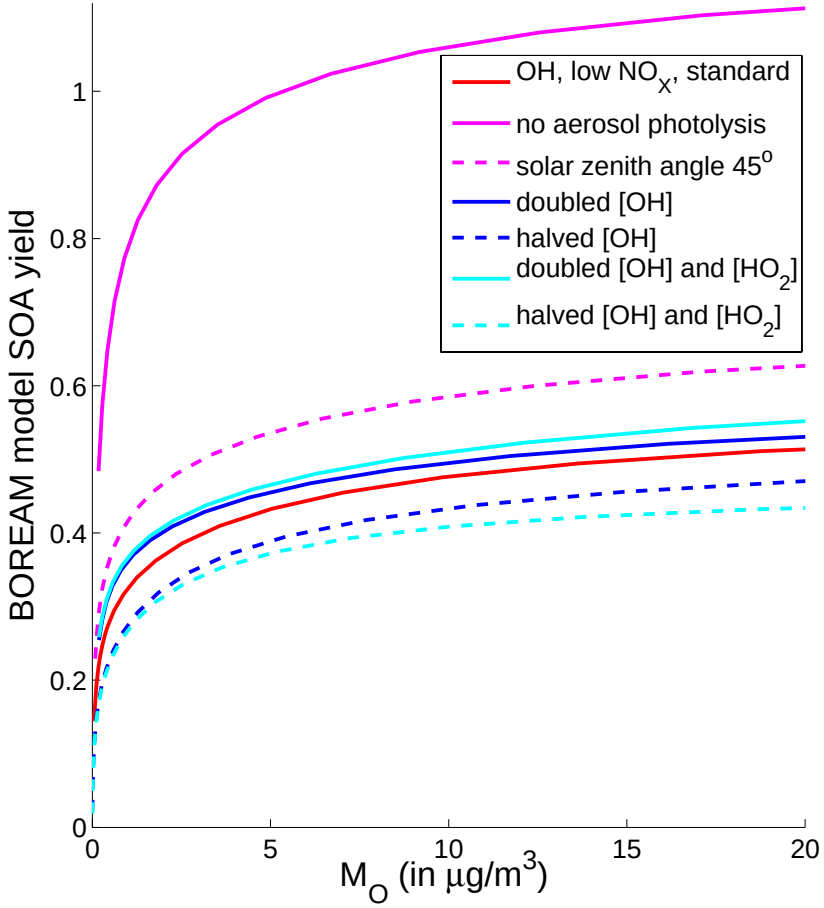

Fig. 5. SOA yields calculated for the OH-oxidation of α-pinene at low-NO_x scenario, at 298 K.

ACPD
11, 23421–23468, 2011

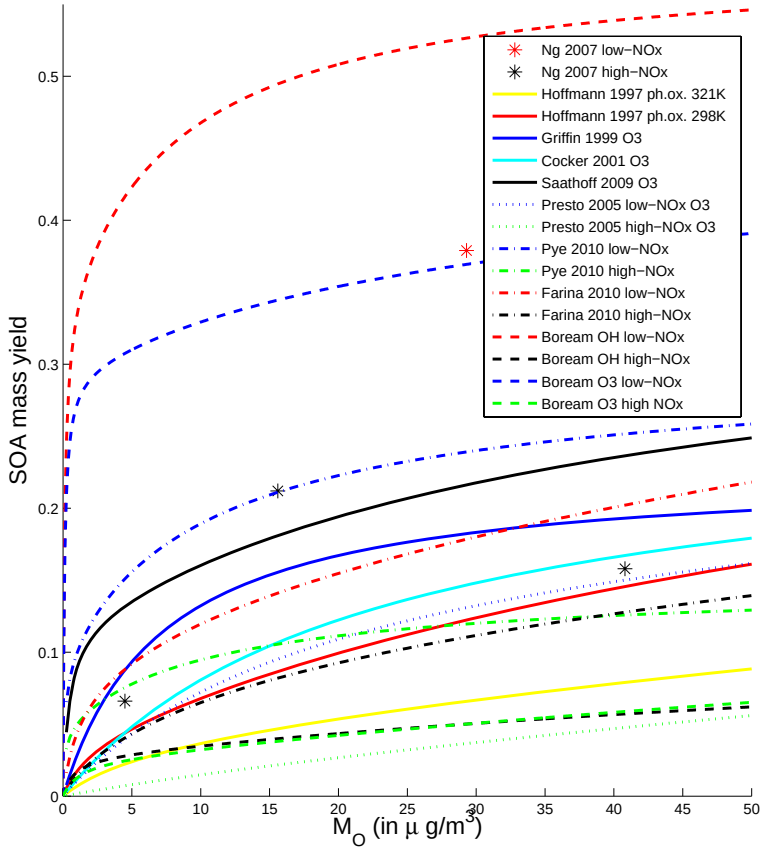

Fig. 6. Comparison of previously derived SOA mass yield curves from other studies, based on smog chamber experiments, with parameterisations based on the BOREAM model (four scenarios, dashed lines). Also shown are the measured experimental yields of Ng et al. (2007a).

ACPD
11, 23421–23468, 2011

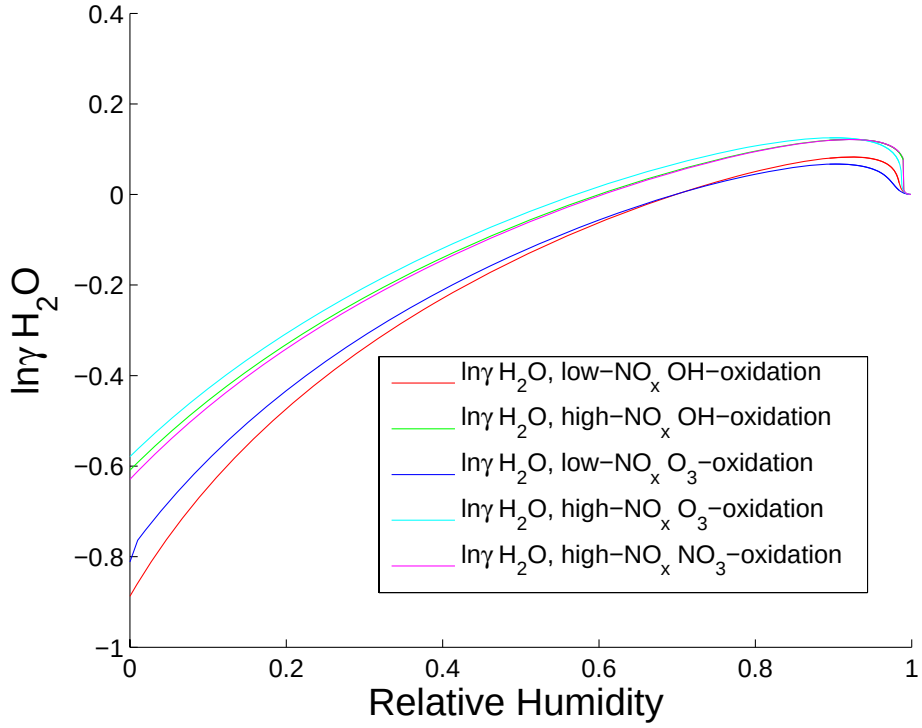

Fig. 7. The activity coefficient of water in function of RH, for the five oxidation scenarios (at 298 K).

ACPD
11, 23421–23468, 2011

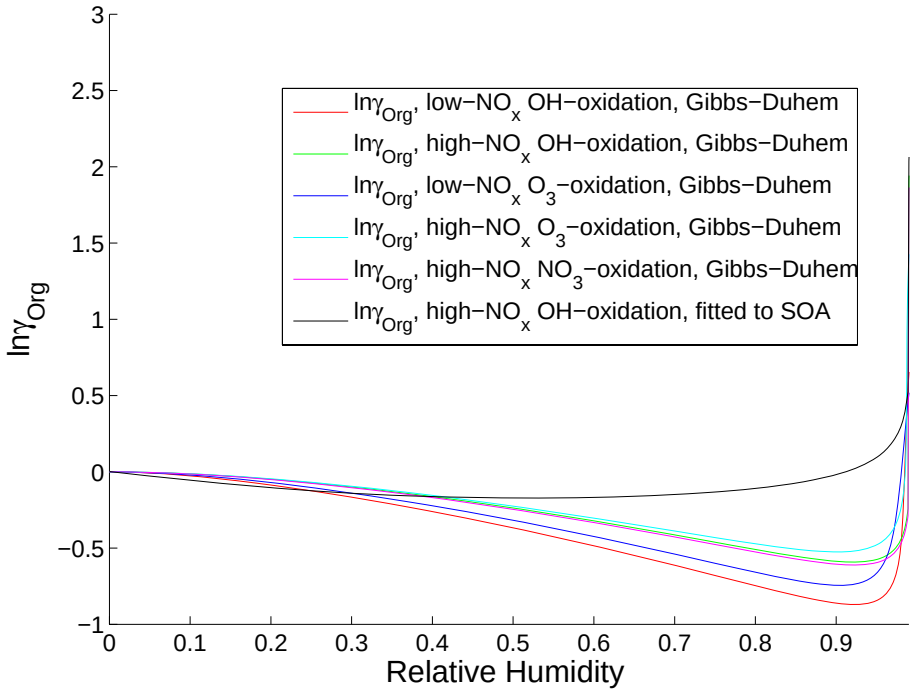

Fig. 8. The pseudo-activity coefficient γ_{Org}, which accounts for the non-ideality effects of water on the organic fraction. It is derived based on the Gibbs-Duhem equation for the 5 scenarios of the 10-product parameter model (coloured curves). Since at high-NO_x, the use of this γ_{Org} based on Gibbs-Duhem leads to a poor agreement between full BOREAM SOA yields and the parameterisation, γ_{Org} values derived from full BOREAM calculations are also derived for that case (black curve).

ACPD
11, 23421–23468, 2011

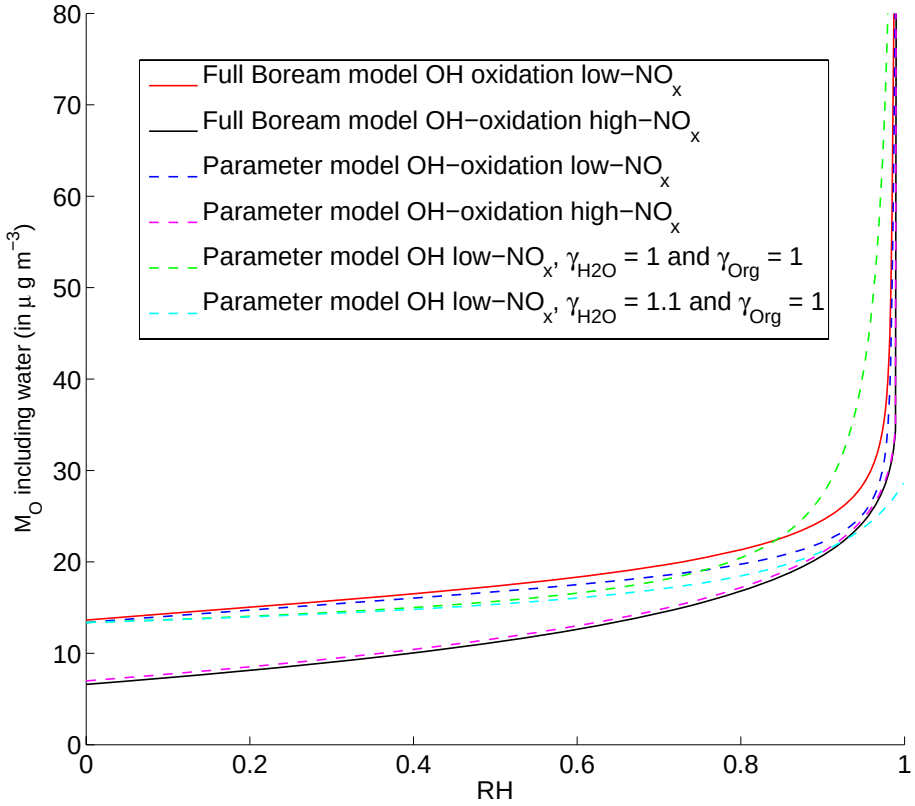

Fig. 9. The impact of relative humidity (RH) on total absorbing mass M_O (including water), for the full model in the case of OH-oxidation at low-NO_x (black) and high-NO_x (blue). The parameter model results are given in red for low NO_x and magenta for high NO_x. Two sensitivity tests illustrate the effect of using constant values for the activity coefficients.

ACPD
11, 23421–23468, 2011